Gas sensing application of nanocrystalline zinc oxide thin films prepared by spray pyrolysis

NISHA R[1,*], K N MADHUSOODANAN[1], T V VIMALKUMAR[2] and K P VIJAYAKUMAR[3]

[1]Department of Instrumentation, Cochin University of Science and Technology, Cochin 682 022, India
[2]Department of Physics, St. Thomas' College, Thrissur 680001, Kerala
[3]Thin Film Photovoltaic Division, Department of Physics, Cochin University of Science and Technology, Cochin 682 022, India

Abstract. Nanocrystalline oxygen-deficient ZnO thinfilm sensors were prepared by spray pyrolysis technique using zinc acetate dissolved in propanol and water as precursor. Response of the sensor to target gases NO_2 and H_2S is studied. At optimum temperature of 200°C, the sensors have a response of 3.32 to 7 ppm NO_2 and 1.4 to 18 ppm of H_2S gas. The analytical characterizations of the prepared sensors were performed using X-ray diffraction measurement, scanning electron microscopy, energy-dispersive X-ray spectroscopy and Raman spectroscopy. Dynamic response of sensors to different concentrations of NO_2 and H_2S gas was tested at optimum temperature. Experimental data revealed the sensors to be more selective to NO_2 gas with satisfactory response and recovery time.

**Keywords.** ZnO; thin film; spray pyrolysis; gas sensor; NO_2; H_2S.

1. Introduction

Monitoring air quality has become a priority due to the great amounts of pollutants released in the atmosphere, which have a toxic effect on ecosystem. To detect pollutant gases different kinds of sensor have been developed, i.e., electrochemical sensors,[1] polymer sensors,[2] surface acoustic wave (SAW) sensors[3] and metal oxide semiconductor (MOS) sensors.[4] The last ones are being preferred mainly because of their simplicity, small dimension and low cost. Conductometric metal oxide gas sensors rely on changes of electrical conductivity due to the interaction with the surrounding atmosphere.[5] In 1991, Yamazoe[6] demonstrated that reduction in crystal size would significantly increase the sensor performance. Nano-sized grains of metal oxides are almost depleted of carriers (most carriers are trapped in surface states) and exhibit much poorer conductivity than micro-sized grains in ambient air; hence, when exposed to target gases, they exhibit greater conductance changes as more carriers are activated from their trapped states to the conduction band than with micro-sized grains. Moreover, the large surface to volume ratio of nanomaterials exhibits high sensitivity to target gases. Hence, in the recent years, researchers are working towards the development of MOS nanomaterial-based sensor elements with improved sensing performance.

ZnO is a material with a variety of potential applications such as electronics,[7] photonics,[8] acoustics,[9] TCO layer in solar cell[10,11] and sensing.[12] On the electronic side, ZnO holds some potential in transparent thin film transistors owing to its high optical transmittivity and high conductivity. In optical emitters, its high exciton binding energy (60 meV)[13] gives ZnO an edge over other semiconductors such as GaN.[14] Due to its large electrochemical coupling, ZnO has significant applications in acoustic wave devices as SAW filter. As a gas sensing material, it is one of the earliest discovered and the most widely applied oxide gas sensing material.[15] ZnO-based elements have attracted much attention as gas sensors because of their chemical sensitivity to different adsorbed gases, high chemical stability, amenability to doping, nontoxicity and low cost. Over the years various researchers have used different forms of ZnO for the detection of many gases. Pure and doped ZnO films prepared by different methods were found to be sensitive to H_2S gas.[16–20] ZnO-based gas sensors were also found to be suitable for detection of gases like methane,[21,22] formaldehyde,[23–25] ethanol,[26–29] ammonia,[30–34] LPG,[35–37] methanol,[38] propanol[38,39] and NO_2.[18,40–44]

In the present context we report the NO_2 and H_2S gas sensing characteristics of oxygen-deficient nanocrystalline zinc oxide films prepared by chemical spray pyrolysis (CSP) technique on glass substrates. Sensor behaviour is presented in detail for a representative concentration for 7 ppm NO_2 and 18 ppm H_2S gas. Gas sensing performance of the sensors to test gases was investigated in the temperature range of 100–225°C.

*Author for correspondence (rnisha.r3@gmail.com)
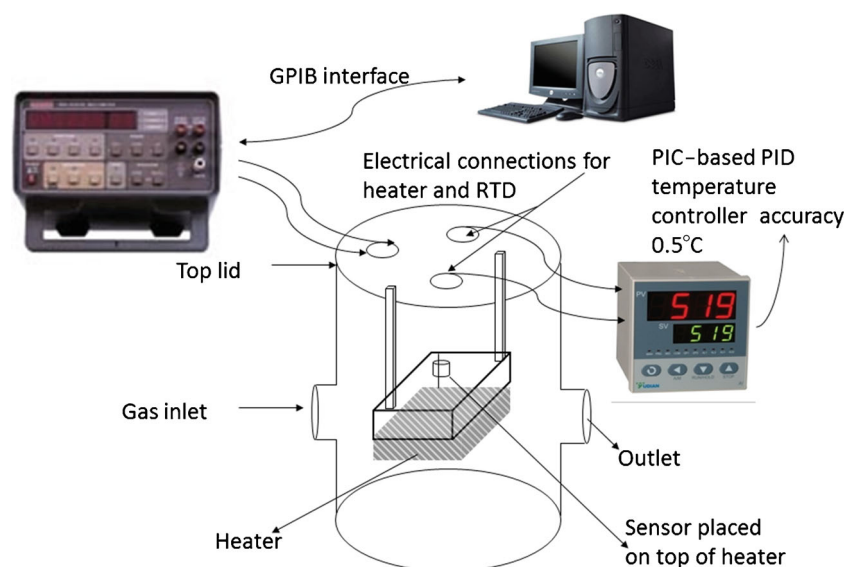
Figure 1. Schematic representation of static test system.

2. Materials and methods

2.1 *Film preparation*

Zinc oxide thin films were prepared on soda lime glass substrate using CSP technique. Zinc acetate solution (0.3 M) was prepared in a mixture of propanol and water, taken in the volume ratio 1:1. This precursor was selected due to its high vapour pressure at low temperature. Addition of few drops of acetic acid prohibits the precipitation of zinc hydroxide, thereby making the spray solution clear and producing films of better optical transmittance. Quantity of acetic acid added to the solution is also a key parameter in the film deposition process. Compressed air was used as the carrier gas (pressure ∼0.34 bar) and temperature of substrate was kept at 450 ± 5°C. Now keeping the molarity of zinc acetate ($Zn(CH_3CO_2)\cdot 2H_2O$) at 0.3 M and spray rate at 7 ml min^{-1}, deposition was done using automated spray machine in which the spray rate, deposition time and movement of the spray head were controlled by a microprocessor. After the deposition, samples were quickly removed from the substrate heater.[45] ZnO films were deposited with ∼550 nm thickness over 30 cm^2 area. ZnO films for gas sensing application were selected after optimizing the various parameters like spray rate, molarity, oxygen stoichiometry and thickness.[46–48] Prior to gas sensing measurements, the films were annealed at an approximate temperature 600°C overnight (Actual temperature at the sample was within a range of 5% of this set temperature.) to remove any possible organic residue remained from the precursor solution and also to improve the crystallinity and to sinter the layer. High temperature annealing also helps in avoiding posterior instabilities, as these sensors are to be operated at elevated temperatures. For the purpose of gas sensing investigations, the films were cut into small pieces with an approximate area of 1 cm^2.

2.2 *Gas sensing measurement setup*

The gas sensing measurements of the thin film sensor were carried out on custom-built static gas characterization system. The schematic representation of test system is shown in figure 1. The test system consists of a stainless steel chamber of diameter 7.5 and 6.35 cm height. The effective volume of the chamber is 280 ml. An inlet is provided for inserting the desired concentration of the gas to the chamber. The gas is injected into the test chamber with a syringe through the inlet provided with septum. Electrical connections from the sensor are taken with the help of two thin copper wires, bonded to the sensor with silver paint. The distance between the two electrodes is adjusted to 5 mm. The sensing capability of the sensor is characterized at different operating temperatures with a precisely controlled heater (±0.5°C) inside the system, to find out the optimum working temperature. Resistance change of the sensor on introduction of the test gas into the chamber is measured using computer-controlled Keithley 195A digital multimeter. Gas concentration is measured by taking required amount of gas from the obtained precalibrated cylinder (Chemtron Science Laboratories) in a syringe and then injecting it into the chamber pre-filled with air at atmospheric pressure. The response of the sensor was studied at different operating temperatures in the range 100–225°C for various concentrations of NO$_2$ and H$_2$S gas ranging from 1.5 to 30 ppm and 5 to 60 ppm in air, respectively.

2.3 *Characterization of the ZnO film*

The crystalline structure and particle size of annealed thin film sensor were examined by X-ray diffraction measurement (XRD, Bruker AXS D8 Advance). Surface morphology of the prepared sensors were analysed using scanning
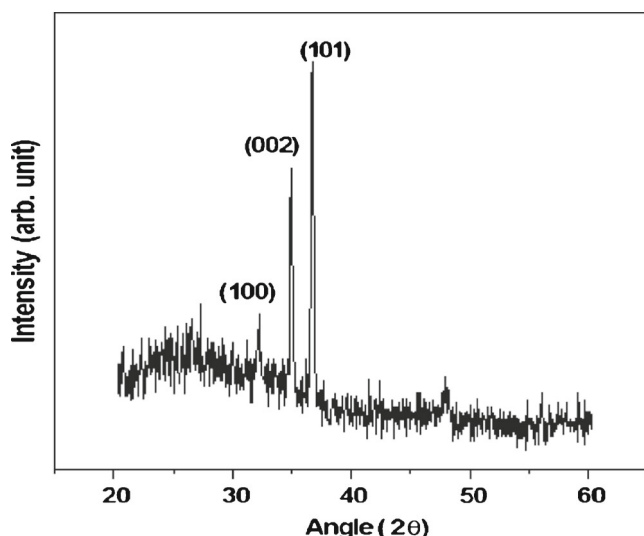
Figure 2. XRD pattern of annealed ZnO thin film sensor.

Figure 3. SEM images of annealed ZnO thin film sensor.

electron microscopy (SEM, JEOL Model JSM-6390LV). Elemental composition of the sensors was performed using energy-dispersive X-ray spectroscopy (EDS, JEOL Model JED-2300). Raman scattering measurements were obtained using Horiba Jobin Yvon LabRam HR system at a spatial resolution of 2 mm in a backscattering configuration. The 514.5 nm line of argon ion laser was used for excitation.
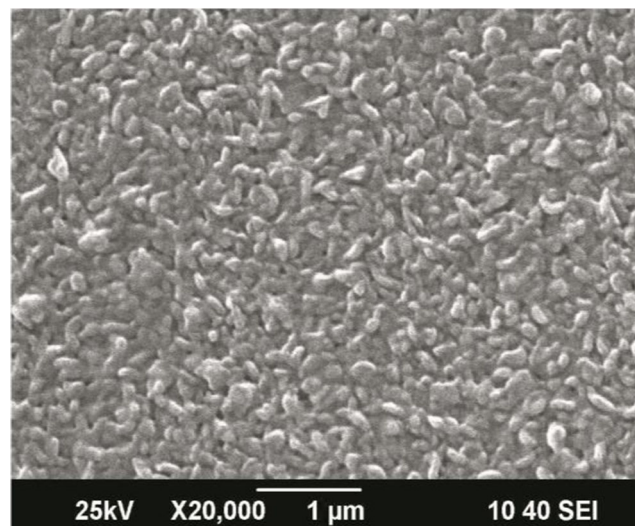
3. Result and discussion

3.1 *XRD*

Crystalline structure analysis of the prepared sensors was performed using XRD. Figure 2 shows the XRD pattern of annealed sensor. All peaks can be confirmed to correspond to the hexagonal wruzite structure of ZnO (JCPDS No. 36-1451). Main reflections were obtained in the (30°–40°) 2θ range corresponding to (100), (002) and (101) planes, the (101) plane being prominent. Under the reactive conditions adopted in our experiments, the ZnO films tend to grow along the maximum density (101) plane. Earlier reports by Fan *et al*[49] proved that the presence of thin film stress can alter the energetic balance between (0 0 2) and (10 1) orientations and lead to preferred (10 1) texture in certain conditions.[49,50]
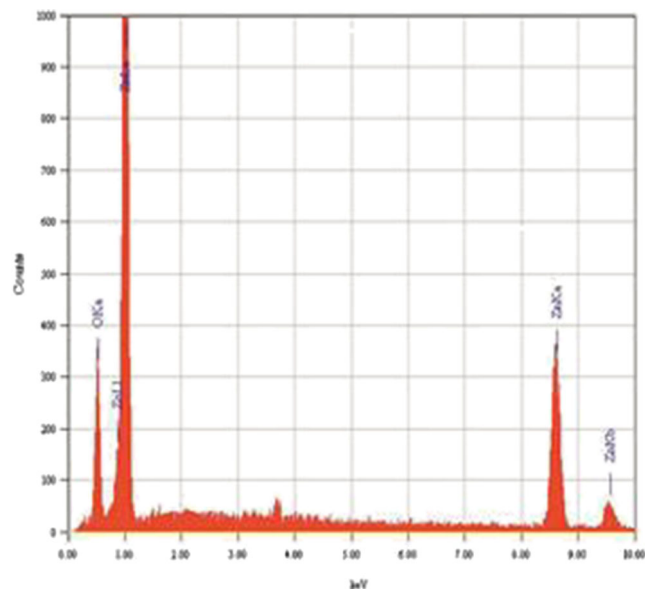
The crystallite size (D) was calculated from peak broadening using the Scherrer approximation, which is defined as

$$D = \frac{0.9\lambda}{B\cos\theta}, \tag{1}$$

where λ is the wavelength of the X-ray (1.5418 Å), B the full-width at half maximum (FWHM, radian) and θ the Bragg angle (degree). The crystallite sizes were calculated using FWHM of the peaks corresponding to the planes (10 0), (0 0 2) and (1 0 1). The average crystallite size was found

Figure 4. EDS spectrum of annealed ZnO thin film sensor.

to be 38 nm. The XRD studies confirmed the nanocrystalline nature of thin film sensor.

3.2 *SEM and EDS*

SEM image of the annealed sensor shown in figure 3 revealed a closely packed arrangement of crystallites. Particles with not much definite shape were revealed in the SEM images of annealed thin film sensor. The EDS analysis of sensor is shown in figure 4. EDS analysis of annealed ZnO film shows that zinc and oxygen are the only detected elements. The SEM image provided a rough representation of the annealed thin film sensor. The EDS analysis performed proved that the prepared sensor film composed of zinc and oxygen

3.3 *Raman spectroscopy*

Raman spectrum of annealed thin film sensor is shown in figure 5. Raman spectroscopy gives information on vibrational properties of ZnO.[51] It is known for wurtzite-type ZnO (space group p6$_3$mc) that optical phonons at the Γ point of the Brillouin zone belong to the following irreducible representation: $\Gamma = A_1 + E_1 + 2E_2 + 2B_1$, where A_1 and E_1 modes are both Raman and infrared active, E_2 modes are Raman active only and B_1 modes are both Raman and infrared inactive (silent modes).[13,52–54] Nonpolar E_2 phonon modes have two frequencies; the low frequency E_2 mode $\left(E_2^{\text{low}}\right)$ and high frequency E_2 mode $\left(E_2^{\text{high}}\right)$. The E_2 modes at low and high frequencies are at 101 and 437 cm^{-1}, respectively. The low frequency E_2 mode $\left(E_2^{\text{low}}\right)$ is associated with vibration of the Zn sublattice, while the high frequency E_2 mode $\left(E_2^{\text{high}}\right)$ is related to the vibration of oxygen atoms.[55,56] E_2^{high} of ZnO is the strongest mode in the wurtzite crystal structure. The strong E_2 (high) mode indicates a good crystallinity.[57] Peak at 556 cm^{-1} is a contribution of the E_1 (LO) mode of ZnO in the case of oxygen deficiency.[58,59] Such a strong intensity of 556 cm^{-1} E_1 mode demonstrates that ZnO thin film sensor is oxygen deficient. These oxygen-deficient sites can enhance the gas sensing properties of thin film sensor. An additional peak is obtained at 330 cm^{-1}. Peak at the same position was reported earlier in literature by various researchers.[60–62] This peak is assigned to possible multiple-phonon-scattering. The above presented results confirmed the ZnO hexagonal wurtzite structure, which is in good agreement with the obtained XRD results.
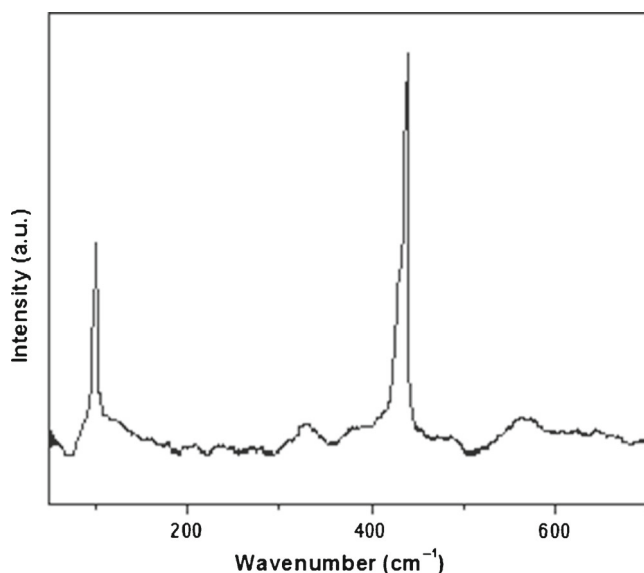
3.4 *Gas sensing investigations*

The gas sensing properties of thin film ZnO sensor was studied in a static gas sensing test system with an effective volume of 280 ml. Sensitivity of the active layer upon oxidizing NO$_2$ gas exposure is measured in terms of the ratio $S = R_{\text{gas}}/R_{\text{air}}$ and for reducing gas (H$_2$S), S is given as $R_{\text{air}}/R_{\text{gas}}$, where R_{gas} is resistance of sensor in presence of gas and R_{air} is resistance of sensor before introduction of gas. The temperature-dependent sensitivity of sensors was studied in the range of 100–225°C. Below the sensor temperature of 100°C, it was difficult to measure gas sensing characteristics due to the sluggish recovery kinetics. Relatively low concentration 7 ppm of NO$_2$ and 18 ppm H$_2$S gas investigation is presented in detail. Similar results were obtained for higher concentration studied. Figure 6a and b represents temperature-dependent sensitivity of sensor to a concentration of 7 ppm NO$_2$ gas and 18 ppm H$_2$S gas studied.

NO$_2$ response of sensor to 7 ppm presents a maximum sensitivity at 200°C as the temperature increases from 100 to 225°C, the sensor sensitivity increasing from 1.22 to 3.32, which is the maximum. Increasing the temperature above
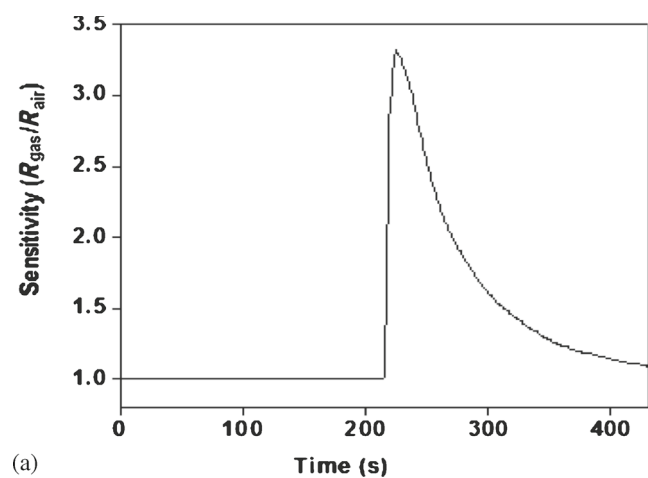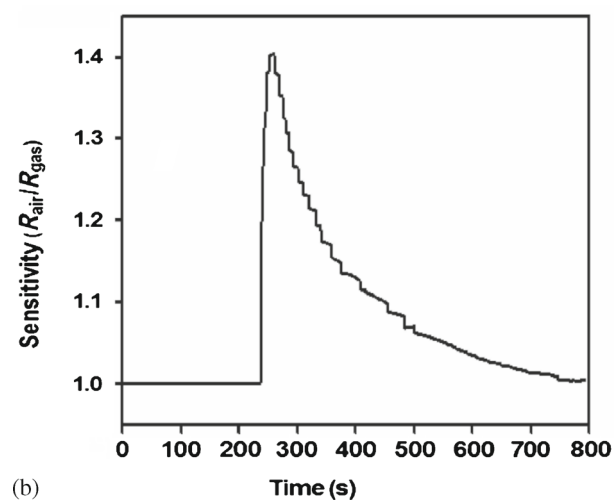

Figure 5. Raman spectra of annealed ZnO thin film sensor.
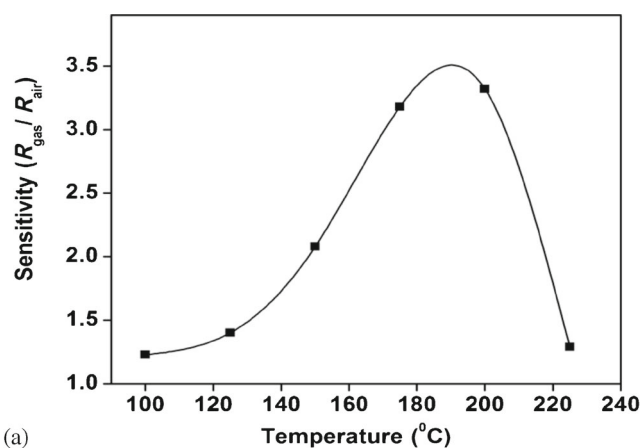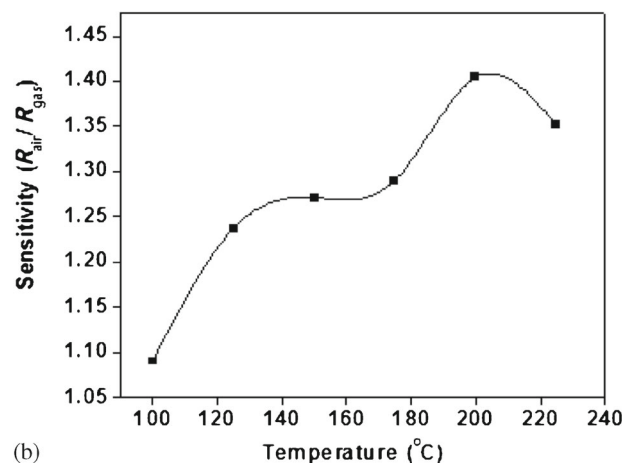
Figure 6. Sensitivity of ZnO thin film sensor towards (**a**) 7 ppm of NO$_2$ gas (**b**) 18 ppm of H$_2$S gas at different temperatures.

200°C decreases sensor sensitivity, achieving 1.29 at 225°C. Concerning the 18 ppm H_2S sensor response, sensitivity increases with increase of temperature in the studied range, attaining a maximum 1.4 at 200°C. Increasing the temperature more than 200°C, the sensitivity decreases and attains 1.15 at 225°C. Considering the temperature-dependent sensitivity studies, optimal operating temperature of 200°C was chosen to further examine the characteristics of the gas sensor to NO_2 and H_2S gas. Comparing the maximum sensitivity values (3.32 for 7 ppm NO_2 and 1.4 for 18 ppm H_2S), ZnO sensor is more sensitive to NO_2 at lower concentration and operating temperature. Figure 7a and b shows response of sensor to 7 ppm NO_2 and 18 ppm H_2S gas at 200°C, respectively.

The maximum sensitivity of ZnO being obtained at 200°C, the dynamic responses of ZnO thin film gas sensor at 200°C were tested with different NO_2 concentrations at 1.5, 3.5 and 30 ppm, respectively. Figure 8 represents the dynamic response of sensor to different NO_2 gas concentration studied. Dynamic responses of the sensor to 5, 10, 30 and 60 ppm concentration of H_2S gas were performed at the

optimum operating temperature of 200°C. Figure 9 represents the dynamic response of the sensor to H_2S gas at 200°C to various concentrations.

Chemoresistivity is the basis of sensing mechanism for metal oxides, which consists of a variation of intergranular and intragranular barriers with subsequent conductance change, as a response to surface chemical reactions with environmental gases. ZnO-based gas elements prepared in nanocrystalline form have large numbers of grain boundaries and necks. The adsorbed oxygen on the grain surface extracts the conduction electrons from near-surface region of the grain, leading to the grain-boundary barriers and the neck barriers.[63] The neck barrier controls the electron conducting channel through the neck and the electron density in the space charge layer at the neck.[64] Therefore the neck barrier
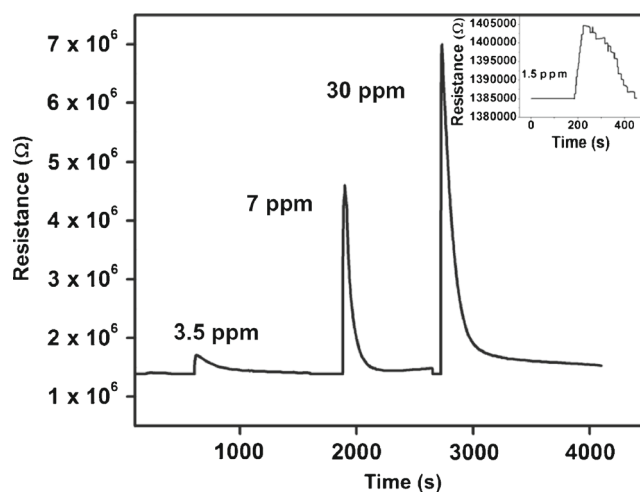
Figure 8. Dynamic response of ZnO thin film sensor to different NO_2 gas concentrations studied.

Figure 7. Response of ZnO thin film sensor to (**a**) 7 ppm NO_2 gas and (**b**) 18 ppm H_2S gas at 200°C.
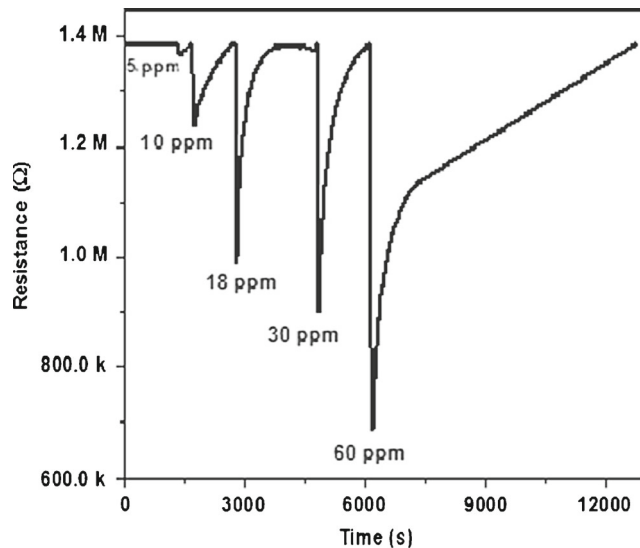
Figure 9. Dynamic response of thin film sensor to different H_2S gas concentrations studied.
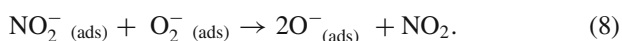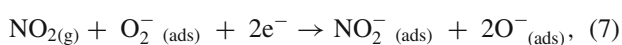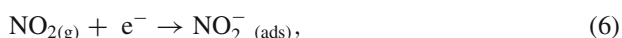
determines the neck resistance. At the same time, the grain-boundary barrier determines the grain-boundary resistance. Ma *et al*[63] studied the effect of grain size on gas sensitivity on ZnO.[65] This group described the total sensitivity in ZnO-based nanocrystalline sensors is the effect of both neck and the neck–grain boundary resistance. Gupta *et al*[65] studied the sensitivity of ZnO-based gas sensors to NO and H_2S gas. The results demonstrate that response of ZnO sensors to H_2S arises from grain boundary only, whereas both grain boundaries and intra-grain resistances contribute towards response to NO. As XRD studies confirmed the nanocrystalline nature, a similar effect is expected in our sensors to NO_2 and H_2S gases. However, detailed investigations like impedance spectroscopy measurements are to be carried out to confirm these findings.

Oxygen vacancies and defects in lattice act as adsorption sites for oxygen and test gases. As the detection of gases originates from interaction of these adsorbed oxygen atomswith gases, maximum (minimum) defect density in (polycrystalline material) yields maximum (minimum) response.[65] Raman spectroscopy performed on our sensors revealed that the thin film sensors prepared are oxygen deficient. These oxygen vacancies in the sensors act as additional sites for gas adsorption, there by enhancing the sensitivity.

Earlier research works conclude, oxygen adsorbed on the surface of oxide gas sensors undergoes the following reactions given by[66] eqs (2–5).

$$O_{2\,(gas)} \leftrightarrow O_{2\,(ads)}, \tag{2}$$

$$O_{2\,(ads)} + e^- \leftrightarrow O_{2\,(ads)}^-, \tag{3}$$

$$O_{2\,(ads)} + 2e^- \leftrightarrow 2O_{(ads)}^-, \tag{4}$$

$$O_{(ads)}^- + e^- \leftrightarrow O_{2\,(ads)}^-. \tag{5}$$

At low temperatures, O_2^- is commonly chemisorbed. At high temperatures, however, O^- and O^{2-} are chemisorbed while O_2^- disappears.[67] The oxygen ionosorption removes conduction electrons and thus lowers the conductance of ZnO.[67] The reactive oxygen species such as O^{2-}, O_2^- and O^- are first adsorbed on ZnO surface when temperature rises. When the sensor film is exposed to NO_2, which is an oxidizing gas, the molecules can be directly adsorbed onto the surface by extracting electrons from the conduction band (eq. (6)) or they can interact with the chemisorbed oxygen on the surface (eqs (7 and 8))
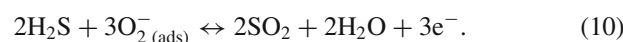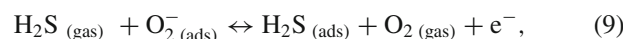
$$NO_{2(g)} + e^- \rightarrow NO_{2\,(ads)}^-, \tag{6}$$

$$NO_{2(g)} + O_{2\,(ads)}^- + 2e^- \rightarrow NO_{2\,(ads)}^- + 2O_{(ads)}^-, \tag{7}$$

$$NO_{2\,(ads)}^- + O_{2\,(ads)}^- \rightarrow 2O_{(ads)}^- + NO_2. \tag{8}$$

As shown in above equations the electrons are consumed in the reactions, which explain the increase of the ZnO resistance after the NO_2 exposure. The adsorption of O_2^- ions is a very interesting and critical phenomenon in metal-oxide gas

sensor, because the O_2^- ions tend to assist the adsorbed NO^{2-} ions in taking the electrons from the ZnO thin films.

The optimum operating temperature for pure and doped sensors was found to be 200°C for NO_2 gas. At lower temperature the sensitivity was low; also the recovery time kept on increasing, which indicates a longer time taken by the sensor to revert back to its base-line properties for the next operation. At low operating temperature sensitivity of the films to NO_2 is restricted by the speed of the chemical reaction, because the electrons do not have enough thermal energy to react with the surface adsorbed oxygen species. In fact, during adsorption of atmospheric oxygen on the film surface, a potential barrier to charge transport is developed. As operating temperature increases the thermal energy obtained is high enough to overcome the potential barrier and thus electron concentration increases significantly, which in turn leads to an increase in sensitivity of sensor films. At optimum operating temperature the sensitivity is maximum. This is attributed to the availability of sufficient adsorbed ionic species of oxygen on film surface, which react most effectively with NO_2 molecules at this particular temperature. The results obtained for NO_2 gas sensing is comparable with earlier published results.[68,69]

A reverse effect is observed when the sensor films are exposed to H_2S gas, a decrease of the ZnO film resistance under H_2S exposure, which can be explained by its reaction with chemisorbed oxygen (eqs (9 and 11)), inducing the release of electrons in the conduction band.[70] The gas response by MOS, in general, can be described as

$$H_2S_{(gas)} + O_{2\,(ads)}^- \leftrightarrow H_2S_{(ads)} + O_{2\,(gas)} + e^-, \tag{9}$$

$$2H_2S + 3O_{2\,(ads)}^- \leftrightarrow 2SO_2 + 2H_2O + 3e^-. \tag{10}$$

This reaction shows an increase in the number of electrons (the reaction infuses electrons into sensing layers), thereby decreasing the sensor resistance. In addition to surface reaction with adsorbed oxygen species, chemical conversion of ZnO with H_2S is another possible reaction mechanism affecting conductivity of ZnO sensor. The chemical conversion of gas sensing materials through the direct reaction with target gas is known to be an important mechanism that changes the conductivity and produces a high sensitivity in several sensing materials of metal oxides. The chemical conversion of CuO nanoparticle to metallic copper sulphide (CuS) has been reported in H_2S sensing by Xue *et al*[71] and formation of AuS by reaction of H_2S on the gold nanoparticles was also reported by Shirsat *et al*[72]. Moreover, various types of complex reactions between ZnO and sulphur compounds (SO_x, H_2S, $(NH_4)_2S$ and so on.) have been reported from surface chemistry studies on ZnO.[73–76] Kim *et al*[77] reported the formation of ZnS on the surface of ZnO on exposure to H_2S gas at a temperature above 300°C. The XPS studies revealed that at temperature above 300°C, beside surface reaction with oxygen, H_2S also decomposes to form Zn-S bonds in ZnO; this change causes the formation of a shallow donor level and causes a drastic increase in conductivity. Wang *et al*[78] studied

the sensitivity of ZnO to H$_2$S gas in the temperature range of 100–450°C and reported the sulphuration of ZnO surface on exposure to H$_2$S gas. When the sensor was exposed to H$_2$S gas, the transformation of highly resistive ZnO into well-conducting ZnS led to the decrease of electrical resistance. The reactions in the response and recovery processes can be represented as follows:

$$ZnO(s) + H_2S(g) \rightarrow ZnS(s) + H_2O(g), \qquad (11)$$

$$2ZnS(s) + 3O_2(g) \rightarrow 2ZnO(s) + 2SO_2(g). \qquad (12)$$
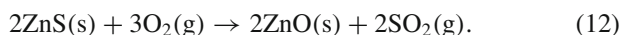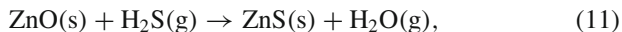
The Gibbs free energy, enthalpy and entropy for both sulphuration and desulphuration were calculated by the group and the results showed that both reactions are spontaneous. We expect the same kind of sulphuration process in our ZnO thin film H$_2$S sensors along with the reaction of H$_2$S with oxygen adsorbates, thereby decreasing sensor resistance in the presence of H$_2$S gas.

Response and recovery times are important parameters for designing sensors for desired application. Response/recovery times are defined as the time required for absorption and desorption of the oxygen on, or from the sensor surface to reach the saturation or to reduce the conductivity back to the baseline conductance. Response time of a sensor can vary from seconds to minutes, but a good sensor is the one that shows a short response and recovery time. In our work, response time of sensor was defined as time required for sensor resistance to reach 90% of maximum resistance. Recovery time was defined as time necessary for the sensor to return to 10% of its original resistance (before introduction of gas). Response and recovery time of ZnO sensor to 7 ppm NO$_2$ and 18 ppm H$_2$S gas at the temperature range of 100–225°C was recorded and is shown in figure 10a and b. At optimum temperature of 200°C, the response time of ZnO sensor was 6 and 10 s to NO$_2$ and H$_2$S gases, respectively. The recovery time recorded was 2.3 and 7 min to NO$_2$ and H$_2$S gases respectively. The response and recovery time obtained for ZnO sensor to NO$_2$ gas is comparable with earlier published results.[44,68,79,80] Compared to NO$_2$ measurements it is seen that the recovery characteristics are very slow for H$_2$S measurements. This may be due to slow desulphuration process on the surface of sensors resulting in larger recovery time.

4. Conclusion

ZnO thin film sensors were fabricated by spray pyrolysis technique. The prepared films were annealed at 600°C overnight prior to gas sensing measurements. The XRD analysis confirmed the nanocrystalline nature of the annealed sensor. The average particle size was found to be 38 nm. The crystalline structure was found to be hexagonal wruzite in nature. Surface morphological studies performed with SEM revealed closely packed arrangement of crystallites. Elemental analysis were performed using EDS. Raman spectroscopy studies confirmed the ZnO hexagonal wurtzite structure. Raman studies established the oxygen deficient nature of thin film sensor, which has an added advantage for gas sensing purposes. Gas sensing investigation of the prepared sensors was characterized with NO$_2$ and H$_2$S gases. Thin film sensors were found to be more selective to NO$_2$ gas at an optimum temperature of 200°C. For a 7 ppm concentration, the sensor sensitivity was 3.32 with a response and recovery time of 6 s and 2.26 min, respectively. It is expected that the response to H$_2$S arises due to changes in grain boundary resistance, while that to NO$_2$ arises due to changes in both intra-grain and grain boundary resistances. Oxygen vacancies in the lattice, as were also seen, enhance the sensor response. However, the exact details of these complicated surface reactions are yet to be fully understood. More detailed experimentation would be necessary to substantiate the suggestions speculated here. The results indicate that spray pyrolysis technique is a reliable method for the preparation of nanocrystalline zinc oxide films for gas sensor applications.
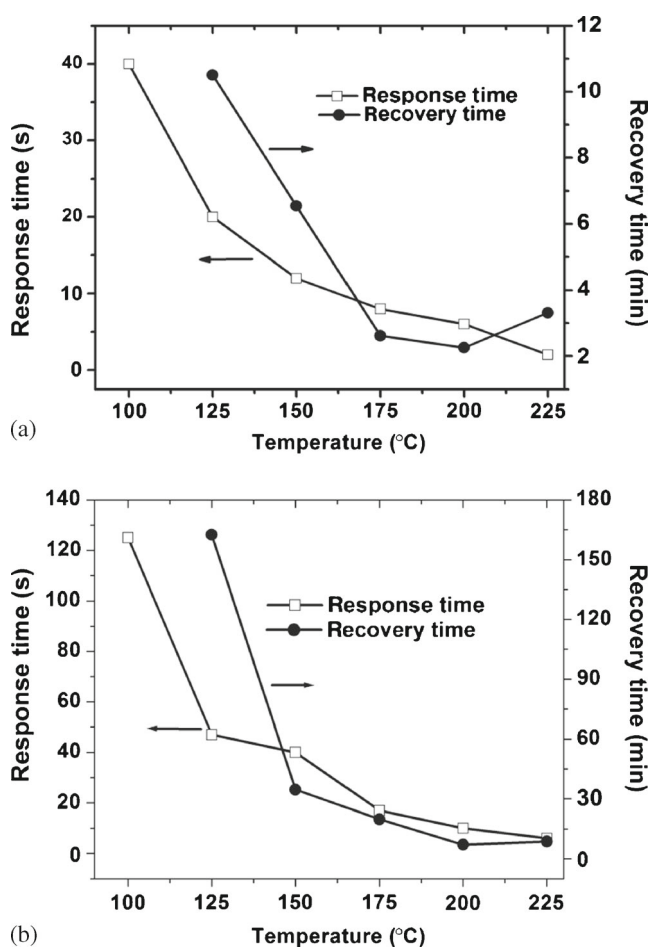
Figure 10. Response and recovery time of ZnO thin film sensor to (**a**) 7 ppm NO$_2$ gas (**b**) 18 ppm H$_2$S gas at different temperature.

References

1. Do J S and Shieh R Y 1996 *Sensors and Actuators B* **37** 19

2. Hoheráková Z and Opekar F 2004 *Sensors and Actuators B* **97** 379

3. Horrillo M C, Fernández M J, Fontecha J L, Sayago I, Garcíá M, Aleixandre M, Gutiérrez J, Gràcia I and Cané C 2006 *Sensors and Actuators B* **118** 356

4. Ionescu R, Hoel A, Granqvist C G, Llobet E and Heszler P 2005 *Sensors and Actuators B* **104** 132

5. Comini E, Faglia G, Sberveglieri G, Pan Z and Wang Z L 2002 *Appl. Phys. Lett.* **81** 1869

6. Yamazoe N 1991 *Sensors and Actuators B* **5** 7

7. Chiou W T, Wu W Y and Ting J M 2003 *Diamond Relat. Mater.* **12** 1841

8. Ibang E J, Le Luyer C and Mugnier J 2003 *Mater. Chem. Phys.* **80** 490

9. Penge W, He Yongning, Wen Changbao and Ke Ma 2012 *Sensors and Actuators A: Physical* **184** 34

10. Baxter J B and Aydil E S 2006 *Sol. Energ. Mater. Sol. Cells* **586** 607

11. Altamirano-Juárez D C, Torres-Delgado G, Jiménez-Sandoval S, Jiménez-Sandoval O and Castanedo-Pérez R 2004 *Sol. Energ. Mater. Sol. Cells* **82** 35

12. Lin F C, Yuji Takao, Yasuhiro Shimizu and Makoto Egashira 1995 *Sensors and Actuators B* **25** 843

13. Özgür Ü, Alivov Y I, Liu C, Teke A, Reshchikov M A, Dogan S, Avrutin V, Cho S J and Morkoc H 2005 *J. Appl. Phys.* **98** 041301

14. Ryu Y R, Kim W J and White J H 2000 *J. Cryst. Growth* **219** 419

15. Seiyama T and Kato A 1962 *Anal. Chem.* **34** 1502

16. Zhang N, Yu K, Li Q, Zhu Z Q and Wan Q 2008 *J. Appl. Phys.* **103** 104305

17. Badadhe S S and Mulla I S 2009 *Sensors and Actuators B* **143** 164

18. Calestani D, Zha M, Mosca R, Zappettini A, Carotta M C, Di Natale V and Zanotti L 2010 *Sensors and Actuators B* **144** 472

19. Ramgir N S, Ghosh M, Veerender P, Datta N, Kaur M, Aswal D K and Gupta S K 2011 *Sensors and Actuators B* **156** 875

20. Shewale P S, Patil V B, Shin S W, Kim J H and Uplane M D 2013 *Sensors and Actuators B* **186** 226

21. Zhou Q, Weigen Chen, Lingna Xu and Shudi Peng 2013 *Sensors* **13** 6171

22. Chen T P, Sheng-Po Chang, Fei-Yi Hung, Shoou-Jinn Chang, Zhan-Shuo Hu and Kuan-Jen Chen 2013 *Sensors* **13** 3941

23. Xie C, Liqi Xiao, Mulin Hu, Zikui Bai, Xianping Xia and Dawen Zeng 2010 *Sensors and Actuators B* **145** 457

24. Chu X, Chen T, Zhang W, Zheng B and Shuia H 2009 *Sensors and Actuators B* **142** 49

25. Han N, Chai L, Wang Q, Tian Y, Deng P and Chen Y 2010 *Sensors and Actuators B* **147** 525

26. Liewhiran C and Phanichphant S 2007 *Sensors* **7** 650

27. Chou S M, Lay Gaik Teoh, Wei Hao Lai, Yen Hsun Su and Min Hsiung Hon 2006 *Sensors* **6** 1420

28. Wang L, Yanfei Kang, Xianghong Liu, Shoumin Zhang, Weiping Huang and Shurong Wang 2012 *Sensors and Actuators B* **162** 237

29. Kim J and Yong K 2011 *J. Phys. Chem. C* **115** 7218

30. Talwar V, Onkar Singh and Ravi Chand Singh 2014 *Sensors and Actuators B* **191** 276

31. Raj V B, Nimal A T, Yashoda Parmar, Sharma M U, Sreenivas K and Vinay Gupta 2010 *Sensors and Actuators B* **147** 517

32. Mani G K and John Bosco Balaguru Rayappan 2013 *Sensors and Actuators B* **183** 459

33. Zeng Y, Zheng Lou, Lili Wang, Zou Bo, Tong Zhang, Weitao Zheng and Guangtian Zou 2011 *Sensors and Actuators B* **156** 395

34. Tulliani J M, Alessio Cavalieri, Simone Musso, Eloisa Sardella and Francesco Geobaldo 2011 *Sensors and Actuators B* **152** 144

35. Ali G M, Cody V T, Ali K J, Isam M A and James C M 2013 *Sensors* **13** 16801

36. Dhawale D S, Dubal D P, More A M, Gujar T P and Lokhande C D 2010 *Sensors and Actuators B* **147** 488

37. Gurav K V, Deshmukh P R and Lokhande C D 2011 *Sensors and Actuators B* **151** 365

38. Prajapati C S and Sahay P P 2011 *Sensors and Actuators B* **160** 1043

39. Huang J, Haibo Ren, Pingping Sun, Cuiping Gu, Yufeng Sun and Jinhuai Liu 2013 *Sensors and Actuators B* **188** 249

40. Chen M, Wang Z, Han D, Gu F and Guo G 2011 *Sensors and Actuators B* **157** 565

41. Hung N L, Kim H, Hong S K and Kim D 2010 *Sensors and Actuators B* **151** 127

42. Rai P, Kim Y S, Song H M, Song M K and Yu Y T 2012 *Sensors and Actuators B* **165** 133

43. Kruefu V, Liewhiran C, Wisitsoraat A and Phanichphant S 2011 *Sensors and Actuators B* **156** 360

44. Chen I C, Shiu-Shiung Lin, Tsao-Jen Lin, Cheng-Liang Hsu, Ting Jen Hsueh and Tien-Yu Shieh 2010 *Sensors* **10** 3057

45. Vimalkumar T V, Poornima N, Sudha Kartha C, Vijayakumar K P, Abe T and Kashiwaba Y 2010a *Physica B* **405** 4957

46. Vimalkumar T V, Poornima N, Sudha Kartha C and Vijayakumar K P 2010b *Appl. Surf. Sci.* **256** 6025

47. Vimalkumar T V, Poornima N, Sudha Kartha C and Vijayakumar K P 2010c *Mater. Sci. Eng. B* **175** 29

48. Vimalkumar T V, Poornima N, Jinesh K B, Sudha Kartha C and Vijayakumar K P 2011 *Appl. Surf. Sci.* **257** 8334

49. Fan X M, Lian J S, Guo Z X and Lu H J 2005 *J. Cryst. Growth* **279** 447

50. Park K S and Park J K 1999 *Acta Mater.* **47** 2177

51. Charpentier C, Prod'homme P, Maurin I, Chaigneau M and Cabarrocas P R 2011 *EPJ Photovoltaics* **2** 25002

52. Minami T, Sato H, Nanto H and Takata S 1984 *Jpn. J. Appl. Phys.* **24** L781

53. Zhou H, Chen L, Malik V, Knies C, Hofmann D M, Bhatti K P, Chaudhary S, Klar P J, Heimbrod W, Klingshirn C and Kalt H 2007 *Phys. Status Solidi A* **204** 112

54. Wang J Z, Peres M, Soares J, Gorochov O, Barradas N P, Alves E, Lewis J E, Fortunato E, Neves A and Monteiro T 2005 *J. Phys. Condens. Matter* **17** 1719

55. Lin K F, Cheng H M, Hsu H C and Hsieh W F 2006 *Appl. Phys. Lett.* **88** 263117

56. Alim K A, Fonoberov V A, Shamsa M and Balandin A A 2005 *J. Appl. Phys.* **97** 124313

57. Lo S S, Huang D, Tu C H, Hou C H and Chen C C 2009 *J. Phys. D: Appl. Phys.* **42** 095420

58. Xu X L, Lau S P and Tay B K 2001 *Thin Solid Films* **398** 244

59. Xu X L, Lau S P, Chen J S, Chen G Y and Tay B K 2001 *J. Cryst. Growth* **223** 201

60. Rajalakshmi M, Arora A K, Bendre B S and Mahamuni S 2000 *J. Appl. Phys.* **87** 2445

61. Damen T C, Porto S P S and Tell B 1966 *Phys. Rev.* **142** 570

62. Calleja J M and Cardona M 1977 *Phys. Rev. B* **16** 3753

63. Ma Y, Wang W L, Liao K J and Kong C Y 2002 *J. Wide Bandgap Mater.* **10** 113

64. Xu C, Tamaki J, Miura N and Yamazoe N 1991 *Sensors and Actuators B* **3** 147

65. Gupta S K, Aditee Joshi and Manmeet Kaur 2010 *J. Chem. Sci.* **122** 57

66. Wang Y, Chen J and Wu X 2001 *Mater. Lett.* **49** 361

67. Kohl D 1990 *Sensors and Actuators B* **1** 158

68. Tamaekong N, Chaikarn Liewhiran, Anurat Wisitsoraat and Sukon Phanichphant 2010 *Sensors* **10** 7863

69. Ghimbeu C M, Joop Schoonman, Martine Lumbreras and Maryam Siadat 2007 *Appl. Surf. Sci.* **253** 7483

70. Arshak K and Gaidan I 2005 *Mater. Sci. Eng. B* **118** 44

71. Xue X, Xing L, Chen Y, Shi S, Wang Y and Wang T 2008 *J. Phys. Chem. C* **112** 12157

72. Shirsat D, Bangar M A, Deshusses M A, Myung N V and Mulchandani A 2009 *Appl. Phys. Lett.* **94** 083502

73. Chaturvedi S, Rodriguez J A, Jirsak T and Hrbek J 1998 *J. Phys. Chem. B* **102** 7033

74. Dloczik L, Engelhardt R, Ernst K, Fiechter S, Sieber I and Konenkamp R 2001 *Appl. Phys. Lett.* **78** 3687

75. Rodriguez J A, Jirsak T, Chaturvedi S and Kuhn M 1999 *Surf. Sci.* **442** 400

76. Uhlrich J J, Franking R, Hamers J and Kuech T F 2009 *J. Phys. Chem. C* **113** 21147

77. Kim K M, Hae-Ryong Kim, Kwon-Il Choi, Hyo-Joong Kim and Jong-Heun Lee 2011 *Sensors* **11** 9685

78. Wang D, Chu X and Gong M 2007 *Nanotechnology* **18** 185601

79. Kim K M, Hyun-Mook Jeong, Hae-Ryong Kim, Kwon-Il Choi, Hyo-Joong Kim and Jong-Heun Lee 2012 *Sensors* **12** 8013

80. Navale S C, Ravia V, Mulla I S, Gosavi S W and Kulkarni S K 2007 *Sensors and Actuators B* **126** 382